Conformational Transitions in p21^{ras} and in Its Complexes with the Effector Protein Raf-RBD and the GTPase Activating Protein GAP†

Matthias Geyer,‡ Thomas Schweins,§ Christian Herrmann,§ Thomas Prisner,|| Alfred Wittinghofer,§ and Hans Robert Kalbitzer*,‡

Max-Planck-Institut für medizinische Forschung, Jahnstrasse 29, 69120 Heidelberg, Max-Planck-Institut für molekulare Physiologie, Rheinlanddamm 201, 44139 Dortmund, and Freie Universität Berlin, Fachbereich Physik, Arnimallee 14, 14095 Berlin, Germany

Received December 4, 1995; Revised Manuscript Received April 12, 1996⊗

ABSTRACT: ^{31}P NMR revealed that the complex of p21^{ras} with the GTP analog GppNHp·Mg^{2+} exists in two conformational states, states 1 and 2. In wild-type p21^{ras} the equilibrium constant $K_1^{(12)}$ between the two states is 1.09. The population of these states is different for various mutants but independent of temperature. The activation enthalpy $\Delta H^{\ddagger}$ and activation entropy $\Delta S^{\ddagger}$ for the conformational transitions were determined by full-exchange matrix analysis for wild-type p21^{ras} and p21^{ras}(S65P). For the wild-type protein one obtains $\Delta H^{\ddagger} = 89 \pm 2$ kJ mol^{-1} and $\Delta S^{\ddagger} = 102 \pm 20$ J mol^{-1} K^{-1} and for the mutant protein $\Delta H^{\ddagger} = 93 \pm 7$ kJ mol^{-1} and $\Delta S^{\ddagger} = 138 \pm 30$ J mol^{-1} K^{-1}. The study of various p21^{ras} mutants suggests that the two states correspond to different conformations of loop L2, with Tyr-32 in two different positions relative to the bound nucleotide. High-field EPR at 95 GHz suggests that the observed conformational transition does not directly influence the coordination sphere of the protein-bound metal ion. The influence of this transition on loop L4 was studied by ^{1}H NMR with mutants E62H and E63H. There was no indication that L4 takes part in the transition described in L2, although a reversible conformational change could be induced by decreasing the pH value. The exchange between the two states is slow on the NMR time scale (<10 s^{-1}); at approximately pH 5 the population of the two states is equal. The interaction of p21^{ras}−triphosphate complexes with the Ras-binding domain (RBD) of the effector protein c-Raf-1, Raf-RBD, and with the GTPase activating protein GAP was studied by ^{31}P NMR spectroscopy. In complex with Raf-RBD the second conformation of p21^{ras} (state 2) is stabilized. In this conformation Tyr-32 is located in close proximity to the phosphate groups of the nucleotide, and the β-phosphate resonance is shifted upfield by 0.7 ppm. Spectra obtained in the presence of GAP suggest that in the ground state GAP does not interact directly with the nucleotide bound to p21^{ras} and does not induce larger conformational changes in the neighborhood of the nucleotide. The experimental data are consistent with a picture where GAP accelerates the exchange process between the two states and simultaneously increases the population of state 1 at higher temperature.

The Ras proteins (p21^{ras})[1] are the products of the H-, K-, and N-ras genes. They are highly conserved GTP-binding proteins which play a crucial role in signal transduction pathways from activated cell surface receptors controlling cell proliferation, differentiation, and metabolism. Ras proteins function as binary switches, cycling between an active GTP and an inactive GDP bound state. Cycling between the two states is mediated by nucleotide exchange and GTP hydrolysis, regulated by guanine nucleotide exchange factors (GEFs) and GTPase-activating proteins (GAPs) [for a review see Boguski and McCormick (1993)]. In resting cells, p21^{ras} is in the inactive form. It is activated through the action of Ras-GEFs such as Sos or Cdc25. In the GTP-bound form, it can interact with its downstream effectors such as the c-Raf protein kinase or PI(3) kinase, which are themselves thereby activated [for reviews see Burgering and Bos (1995), Wittinghofer and Herrmann (1995), and Lowy and Willumsen (1993)]. It returns to the inactive state via the GTP hydrolysis reaction, which is intrinsically rather slow but can be accelerated by 5 orders of magnitude by GTPase-activating proteins (GAPs) (Gideon et al., 1992; Eccleston et al., 1993). In a large number of human tumors, single point mutations in ras genes have been found at positions 12, 13, and 61 (Barbacid, 1987). The mutant proteins are permanently activated, producing a permanent signal since the intrinsic and the GAP-stimulated GTPase activities are strongly reduced.

The three-dimensional structures of wild-type p21^{ras} (H-ras isoform) in the GDP- and GTP-bound forms and of various oncogenic and nononcogenic mutants have been

† The data were presented at the European Research Conference "NMR in Molecular Biology", Wildbad Kreuth, Germany, 1995.

* To whom correspondence should be addressed.

‡ Max-Planck-Institut für medizinische Forschung, Abteilung Biophysik.

§ Max-Planck-Institut für molekulare Physiologie, Abteilung Strukturelle Biologie.

|| Freie Universität Berlin, Fachbereich Physik.

⊗ Abstract published in *Advance ACS Abstracts,* July 15, 1996.

[1] Abbreviations: NMR, nuclear magnetic resonance; EPR, electron paramagnetic resonance; p21^{ras}, protein product of the H-ras protooncogene; Raf-RBD, Ras binding domain of the Ras effector molecule c-Raf-1; GAP, GTPase activating protein; Rap1A, Ras homolog protein; GppNHp, guanosine 5′-*O*-(β,γ-imidotriphosphate); GppCH$_2$p, guanosine 5′-*O*-(β,γ-methylenetriphosphate); GTPγS, guanosine 5′-*O*-(3-thiotriphosphate); caged GTP, *P*^{3}-[1-(2-nitrophenyl)ethyl]guanosine 5′-*O*-triphosphate; DSS, 2,2-dimethyl-2-silapentane-5-sulfonate; DTE, dithioerythritol; EDTA, ethylenediaminetetraacetic acid; TOCSY, total correlation spectroscopy.

S0006-2960(95)02858-3 CCC: $12.00

analyzed in great detail by X-ray crystallography (Pai et al., 1989, 1990; Milburn et al., 1990; Privé et al., 1992; Franken et al., 1993; Krengel et al., 1990; Scheidig et al., 1995). Structural information on p21−nucleotide−metal complexes has also been obtained by EPR spectroscopy (Feuerstein et al., 1987; Smithers et al., 1990; Latwesen et al., 1992; Larsen et al., 1993) and by ^{31}P NMR spectroscopy (Klaus et al., 1986; Rösch et al., 1986; John et al., 1989; Campbell-Burk, 1989; Grand et al., 1989; Franken et al., 1993). Structural studies on p21^{ras} and its mutants were performed using ^{1}H NMR spectroscopy (Longo et al., 1988; Yamasaki et al., 1989; Ha et al., 1989; Campbell-Burk, 1989; Hata-Tanaka et al., 1989; Schlichting et al., 1990a; Miller et al., 1992/1993; Yamasaki et al., 1994), and complete assignments for isotope-enriched p21^{ras}·GDP and calculations of the solution structures of this complex have been reported recently (Muto et al., 1993; Kraulis et al., 1994).

Magnetic resonance methods can provide detailed dynamic aspects of a protein which are mostly lost in crystal structures where a preferred conformation is frozen out due to crystal packing forces. For an understanding of the function of a protein it is important to evaluate these dynamic processes. A further important goal is to understand the chemical and kinetic mechanism of the GTPase of p21^{ras} and other GTP-binding proteins, which are presumed to be closely related. From fluorescence measurements it has been postulated that the rate-limiting step of the intrinsic GTPase is a conformational change (Neal et al., 1990; Moore et al., 1993), although other authors find the actual cleavage reaction to be the rate-limiting step (Rensland et al., 1991). Recently, we could show that the intrinsic GTP hydrolysis can be explained satisfactorily by a specific acid−base mechanism with the γ-phosphate group of the nucleotide as the primary proton acceptor group (Schweins et al., 1995).

The mechanism of GAP activation of the p21^{ras} GTPase activity is a subject of intense discussion. Two classes of mechanism are in principle imaginable (Lowe & Skinner, 1994; Wittinghofer et al., 1993). In principle, one or more side chains of the GAP molecule could complement the active site of p21^{ras} and thereby accelerate the GTPase reaction, since various conserved residues in Ras-GAP have been found to be important for its activity (Skinner et al., 1991; Wiesmüller & Wittinghofer, 1992; Brownbridge et al., 1993; Gutmann et al., 1993). In the extreme case, this would imply that the chemical mechanism of GTP hydrolysis by GAP-activated p21^{ras} is different from that in p21^{ras} alone. In the other scenario the basic mechanism of catalysis is the same as in p21^{ras} alone, and the role of GAP is to stabilize a certain catalytic active conformation of p21^{ras} or to accelerate the isomerization reaction (Moore et al., 1993). It will be interesting to see what conformational changes occur at the nucleotide binding site due to the interaction of p21^{ras} with the effector molecule Raf kinase. It has been reported that the GTPase activity is not affected, but the nucleotide dissociation strongly inhibited, in the Ras·Raf complex (Herrmann et al., 1995).

In this paper we report magnetic resonance results on the p21^{ras} complexes with different nucleotides and in the complex with the Raf-RBD and the catalytic domain of p120-GAP, which might be relevant to these questions.

MATERIALS AND METHODS

Protein Purification and Sample Preparation. p21^{ras} proteins were expressed in *Escherichia coli* and purified as described before (Tucker et al., 1986) and converted to the GTP form as described (John et al., 1989). The final purity of the proteins was >95% as judged from sodium dodecyl sulfate−polyacrylamide gel electrophoresis. The tightly bound nucleotide GDP was exchanged for the slowly hydrolyzing GTP analog GppNHp according to John et al. (1990). Excess nucleotide and phosphate ions were removed by gel filtration. The protein concentration was determined with the Bradford assay using bovine serum albumin as standard (Bradford, 1976). The amount of protein-bound nucleotide was analyzed with C18 reverse-phase HPLC and quantitated with a calibrated detector (Beckman) and integrator (Shimazu), respectively.

GAP-334 (Gapette) was expressed in *E. coli* and purified as described before (Gideon et al., 1992). The Ras-binding domain of human c-Raf-1 (Raf-RBD, 81 residues) was expressed in *E. coli* and purified as described recently (Herrmann et al., 1995).

Preparation of the NMR Samples. ^{31}P NMR spectra of p21^{ras} complexed with G nucleotides were recorded in 40 mM Hepes, 10 mM $MgCl_2$, and 0.1 mM DTE. Usually, 2.5 mL of the sample was placed in 10 mm NMR tubes (Wilmad) with a protein concentration of 0.4−1.2 mM. To provide a lock signal, the samples contained between 10% and 99% D_2O. For some experiments the sample had to be freeze-dried and redissolved in D_2O. Here, care was taken that the sample was kept permanently at low temperature (liquid nitrogen) and that the freeze-drying process was as short as possible. The protein-free nucleotide samples contained approximately 10 mM nucleotide (GDP, GTP, or GppNHp) in the above buffer but with 30 mM $MgCl_2$ in solution. For experiments on p21^{ras} complexes with GAP or Raf-RBD, usually 1 mM p21^{ras} and highly concentrated GAP (0.7 mM) or Raf-RBD (3.4 mM) solutions were added.

NMR Spectroscopy. ^{31}P and ^{1}H NMR experiments were performed on a Bruker AMX-500 NMR spectrometer working at a proton resonance frequency of 500 MHz and a phosphorus resonance frequency of 202 MHz. Additional phosphorus spectra were recorded on a Bruker AMX-600 and a Bruker HX-360 spectrometer at 243 and 146 MHz, respectively. The ^{31}P spectra were referenced to 85% phosphoric acid contained in a glass sphere which was immersed in the sample and calibrated for various temperatures. Unless noted otherwise, phosphorus spectra were collected at 5 °C with a total spectral width of 60 ppm (100 ppm for samples containing GTPγS).

For one-dimensional ^{31}P NMR spectra, 512−8192 free induction decays were summed after excitation with a 65° pulse using a repetition time of 3−5 s. Most experiments were run in D_2O solution in order to suppress undesired proton phosphorus couplings. A total of 32 K time domain data points were recorded and transformed to 16K real data points corresponding to a digital resolution of 0.74 Hz/point. ^{1}H NMR spectra were recorded with selective presaturation of the water resonance for 1.5 s. All spectra were processed on a Bruker X32/3 workstation with the UXNMR standard software. Spectra used for the complete line-shape analysis were filtered by an exponential window function causing no significant line broadening. The spin−spin coupling constants of the nucleotide−Mg^{2+} complexes were determined from a line fit (see below) of a nonfiltered 1D spectrum with a digital resolution of 0.25 Hz/point after Fourier transformation.

Preparation of the EPR Samples and EPR Spectroscopy. The p21^{ras}·GppNHp·Mn^{2+} complex was generated by incubation of p21·GppNHp·Mg^{2+} with 40 mM ammonium sulfate and 100 mM $MnCl_2$ for about 60 min. Excess metal ions were removed by gel filtration with PD-10 columns (Pharmacia). All buffers used were equilibrated with a chelating resin (Chelex 100, Bio-Rad) to remove traces of bivalent metal ions. DTE (10 mM) was added to the buffer to prevent oxidation of the protein and of Mn^{2+}. To ensure that the Mg^{2+} ion is replaced quantitatively by Mn^{2+}, the exchange process was repeated twice. EPR spectra were recorded with a home-built high-field spectrometer operating at 95 GHz and 3.4 T, respectively (Prisner et al., 1994). The spectra were measured in the cw mode with a microwave power of 1 μW and a modulation amplitude of 0.1 mT. Protein concentration was in the range 1.0−1.5 mM in 50 mM Tris-HCl buffer of pH 7.4.

Determination of Exchange Rates. The NMR spectra were evaluated with a simulation software written in our laboratory. The software package is written in C and runs on UNIX workstations. The simulated spectra were displayed and plotted with the program UXNMR from Bruker, Karlsruhe.

The two-site exchange was simulated on the basis of the full-density matrix formalism as described by Kaplan & Fraenkel (1980) and Nageswara Rao (1989). For triphosphate nucleotides the system can be described as

$$\underset{1}{\mathrm{ABC}} \underset{k_{-1}}{\overset{k_1}{\rightleftharpoons}} \underset{2}{\mathrm{A'B'C'}} \tag{1}$$

with ABC the α-, β-, and γ-phosphate in state 1 and A′B′C′ the phosphate groups in state 2 and k_1 and k_{-1} the rate constants for this process. For a description of this process the populations p_1 and p_2 of states 1 and 2 must be known. The equilibrium constant K is given by

$$K = k_1/k_{-1} = p_2/p_1 \tag{2}$$

NMR parameters entering the calculation are the spin $I = {}^1/_2$ of ^{31}P, the resonance frequences ν_A, ν_B, ν_C, $\nu_{A'}$, $\nu_{B'}$, and $\nu_{C'}$, the coupling constants J_{AB}, J_{BC}, J_{AC}, $J_{A'B'}$, $J_{B'C'}$, and $J_{A'C'}$, and the transverse relaxation times $T_{2,A}$, $T_{2,B}$, $T_{2,C}$, $T_{2,A'}$, $T_{2,B'}$, $T_{2,C'}$.

The *J*-coupling constants in the protein-bound state cannot be obtained directly, since they are not resolved in the spectra. They were approximated by the *J*-couplings in the corresponding free nucleotide−Mg^{2+} complexes which can be obtained experimentally. The small changes in these constants that are possible in the bound state can only marginally influence the observed results. The ^{31}P resonance frequencies were obtained by fitting the corresponding p21−nucleotide spectrum recorded at the lowest temperature where slow exchange conditions prevail. Here, a gradient fit procedure, using the Marquardt method [see, e.g., Press et al. (1986)], was performed to determine the mean half-width, the signal amplitude, and the line position of the overlapping peaks by assumption of the *J*-coupling constants and Lorentzian lineshapes. From these parameters the populations p_1 and p_2 in the different states can be derived. As is usual for the simulation of temperature dependence of exchange spectra, it was assumed that the *J*-couplings, the equilibrium constant K, and the resonance frequencies ν_j do not vary much with the temperature and can be considered as constant for the following line-shape analysis.

The most difficult parameters to obtain are the transverse relaxation times T_2 since they are temperature dependent and since it is difficult to determine them in the presence of exchange broadening. In principle, they can be obtained for extreme temperatures with $|2\pi\ \Delta\nu| \gg 1/\tau_e$ or $|2\pi\ \Delta\nu| \ll 1/\tau_e$ directly from the line widths. This method, which is commonly applied in physical chemistry, fails in our case since the extreme temperatures necessary cannot be obtained without denaturation of the protein or freezing of the sample. However, a lower limit on the T_2's can be obtained with the assumption that at the lowest temperature measured exchange broadening is negligible. Since the transverse relaxation time should increase with temperature (assuming relaxation via dipolar interaction and chemical shift anisotropy in a rigid body model), the lower limit obtained holds for the whole temperature range.

The principal functional form of the temperature dependence of the relaxation rates depends on the relaxation mechanisms involved. Since this temperature dependence represents only a small correction term in the calculation of the exchange rates, it is sufficient to assume only relaxation via dipolar interaction and chemical shift anisotropy and isotropic rotational reorientation with the correlation time τ_r. The transverse relaxation rates for the phosphorus nucleus x (x = A, B, C, A′, B′, C′) can be written as

$$\frac{1}{T_2^x} = \frac{\mu_0}{4\pi^2}\frac{\hbar^2\gamma_x^2}{20}\sum_{j\neq x}\frac{\gamma_j^2}{r_{xj}^6} f_{DD}(\tau_r,\omega_x,\omega_j) + \frac{2}{15}\gamma_x B_0^2 \Delta\sigma^2 f_{CSA}(\tau_r,\omega_x) \tag{3}$$

with μ_0 the vacuum permeability, γ_x the phosphorus magnetogyric ratio, γ_j the proton or phosphorus magnetogyric ratio, and r_{xj} the distance between spins x and j. For proteins of the size of p21^{ras}, functions f_{DD} and f_{CSA} can be assumed to be approximately proportional to τ_r. As long as the environment of the spin x does not change with the temperature, eq 3 can be simplified to

$$\frac{1}{T_2^x} = c_x\tau_r \tag{4}$$

with c_x a constant characterizing the environment of spin x. For isotropic rotation τ_r is given by the Stokes−Einstein relation

$$\tau_r = V'\frac{\eta}{kT} \tag{5}$$

with η the viscosity of the solution and V' the effective volume of the molecule. The temperature dependence of the viscosity of aqueous solution can be described by

$$\eta = Ae^{-b/T} \tag{6}$$

with A and b empirical constants. These constants were determined from viscosity data of H_2O and D_2O tabulated, e.g., in Landolt-Börnstein (1969). A fit to the data in the range from 273 K (e.g., 277 K) to 313 K results in A = 1.737 g m^{-1} s^{-1}, b = 0.0262 K for H_2O and A = 2.279 g m^{-1} s^{-1}, b = 0.0285 K for D_2O. From eqs 4−6 it follows

that

$$\frac{1}{T_2^x} = c_x \frac{V' A}{kT} e^{-b/T} \quad (7)$$

The simulation of the spectra and the calculation of the parameters were performed iteratively. First, for the lowest temperature spectrum the upper limit of the exchange rate k_{max} was determined for slow exchange. For a grid of rate constants in the range between 0 and k_{max} the transverse relaxation times for the different resonances were calculated. Starting with these values the complete temperature series was fitted assuming the temperature dependence given by eq 7. By visual inspection of the measured and simulated spectra the range of possible exchange rates at the lowest temperature could be narrowed down considerably. Within this range the simulation parameters were refined iteratively until the optimal solution had been found.

The temperature dependence of the rate constants was fitted with the program Grafit (Erithacus Software) on the basis of transition state theory (Eyring, 1935) to the equation

$$k_1 = \kappa \frac{kT}{h} e^{-(\Delta H^{\ddagger} - T\Delta S^{\ddagger})/RT} \quad (8)$$

where κ is the transmission coefficient, k the Boltzmann constant, h the Planck constant, R the gas constant, T the absolute temperature, $\Delta H^{\ddagger}$ the activation enthalpy, and $\Delta S^{\ddagger}$ the activation entropy.

RESULTS

^{31}P NMR Spectra of the p21·GppNHp·Mg^{2+} Complex. The phosphorus NMR spectra of triphosphates bound to proteins with a single nucleotide binding site usually show only three resonances, corresponding to the α-, β-, and γ-groups of the complexed nucleotide. Published ^{31}P NMR spectra of p21−nucleoside triphosphate complexes (Klaus et al., 1986; Rösch et al., 1986; John et al., 1989; Campbell-Burk, 1989; Grand et al., 1989; Franken et al., 1993) as well as the spectra we recorded at room temperature correspond to this scheme. In contrast, additional phosphorus resonance lines become visible in the spectra of the p21·GppNHp·Mg^{2+} complex at lower temperatures (Figure 1). The line widths and line positions exclude the possibility that these lines arise from free nucleotide. Therefore, they must result from different states, states 1 and 2, of the nucleotide bound to the protein. A closer inspection suggests that the resonance lines of the different phosphate groups split in two lines. This is most obvious for the resonance of the β-phosphate but is also visible as inhomogeneity of the α-phosphate line. Only the γ-phosphate line appears to be unperturbed. A careful integration of fully relaxed spectra shows that the integral of the γ-phosphate line equals that of the sum of the two β-phosphate lines or the α-phosphate lines. The data are consistent with the assumption of two states of the nucleotide−protein complex with α-resonances at slightly different positions, β-lines at clearly different positions, and γ-lines at the same positions. An increase in temperature leads to a coalescence of lines as is typical for a two-site exchange with a transition from slow exchange to fast exchange. This process is completely reversible, the initial spectrum essentially returning when the temperature was lowered (Figure 1). This behavior also excludes the possibility that one of the two states corresponds to nucleotide binding to irreversibly denatured protein.

A possible explanation for the observation of the two states could be that, under our experimental conditions, the nucleotide is complexed with magnesium in one of the states and not in the other. Although this is very unlikely from the known binding constants for divalent ions to p21, it was checked experimentally. In the range of 0.1−100 mM free Mg^{2+} in solution no spectral changes were observed. This excludes the possibility that the partial occupancy of the high-affinity site of p21 or a possible low-affinity binding site for Mg^{2+} is responsible for the observed line splitting. The line splitting and the relative intensities (populations) of the lines are not dependent on pH in the range from 6.5 to 10.4.

^{31}P NMR Spectra of the p21·GppNHp·Mg^{2+} Complex in Mutant Proteins. To check whether the observed conformational equilibrium is a special property of wild-type

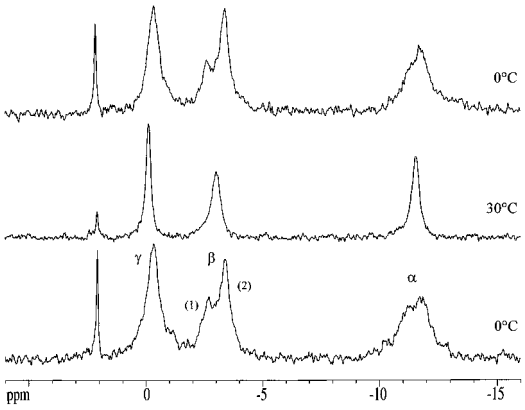

FIGURE 1: ^{31}P NMR spectra of p21^{ras}·GppNHp·Mg^{2+} at different temperatures: 0.7 mM wild-type p21^{ras} complexed with GppNHp and 2.0 mM $MgCl_2$ in D_2O, pH 7.4. (Bottom) Spectrum at 0 °C, recorded before the high-temperature spectrum (Middle) of 30 °C. (Top) Temperature 0 °C, recorded after the high-temperature spectrum.

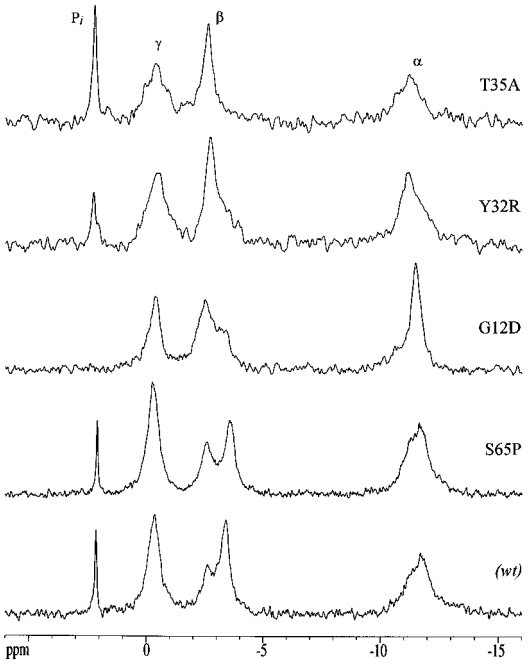

FIGURE 2: ^{31}P NMR spectra of wild-type and mutant p21^{ras} complexes with GppNHp·Mg^{2+}. Spectra were recorded at 5 °C and pH 7.4. Protein concentrations were wild type, 0.7 mM; S65P, 0.8 mM; G12D, 0.7 mM; Y32R, 0.4 mM; T35A, 0.4 mM; all with 10 mM free Mg^{2+}. Note that the number of scans for each spectrum varied.

Table 1: ^{31}P NMR Chemical Shifts of Different p21^{ras}−Nucleoside Triphosphate Complexes[a]

complex	chemical shifts δ (ppm)[b]						equilibrium constant $K_1^{(12)}$[c]
	$\alpha^{(1)}$	$\alpha^{(2)}$	$\beta^{(1)}$	$\beta^{(2)}$	$\gamma^{(1)}$	$\gamma^{(2)}$	
p21(wt)·GppNHp·Mg^{2+}	−11.15	−11.85	−2.69	−3.41	−0.41	−0.23	1.09
p21(G12D)·GppNHp·Mg^{2+}	−11.49		−2.47	−3.39	−0.36		0.52
p21(Y32R)·GppNHp·Mg^{2+}	−10.98		−2.53		−0.23		<0.2
p21(T35A)·GppNHp·Mg^{2+}	−11.09		−2.51		−0.25		<0.05
p21(E62H)·GppNHp·Mg^{2+}	−11.21	−11.82	−2.60	−3.42	−0.38	−0.24	1.0
p21(S65P)·GppNHp·Mg^{2+}	−11.28	−11.78	−2.58	−3.59	−0.37	−0.23	1.0
p21(S65P)·GppNHp	−10.85		−3.95		−1.45		−[d]
p21(wt)·GTP·Mg^{2+}	−11.77		−14.97	∼−15.7	−7.99		<0.1
p21(G12V)·GTP·Mg^{2+}	−11.76		−14.94		−7.72		
p21(Q61H)·GTP·Mg^{2+}	−11.84		−14.93	−15.73	−7.81		0.21
p21(Q61L)·GTP·Mg^{2+}	−11.67		−14.70	−15.81	−7.73		0.23
p21(Q61P)·GTP·Mg^{2+}	−11.71		−15.10		−7.75		
p21(S65P)·GTP·Mg^{2+}	−11.74		−14.96		−8.31		
p21(Q61H)·GTP	−11.27		−16.53		−5.24		−[d]
p21(wt)·GTPγS·Mg^{2+}	−11.30		−16.62		37.01		

[a] Experimental conditions as in Figures 1 and 2. Usually spectra were recorded at 5 °C and pH 7.4. [b] The resonances of states 1 and 2 are designated as $\alpha^{(1)}$, $\alpha^{(2)}$, $\beta^{(1)}$, $\beta^{(2)}$, $\gamma^{(1)}$, and $\gamma^{(2)}$. State 1 is defined as the state where the β-resonance is shifted downfield relative to the second β-resonance. Chemical shift values tabulated for both $\gamma^{(1)}$- and $\gamma^{(2)}$-resonances were obtained by line-shape deconvolution. [c] The equilibrium constant $K_1^{(12)}$ is calculated from the integrals of the β-resonances of the two states, 1 and 2, and is defined by $K_1^{(12)} = k_1^{(12)}/k_{-1}^{(12)} = [(2)]/[(1)]$. [d] The data were obtained by removing the protein-bound Mg^{2+} by addition of EDTA to the solution. The spectral quality at 5 °C was not sufficient to decide if a second state also exists in absence of Mg^{2+}. The values given for p21(S65P)·GppNHp are measured at 25 °C.

protein and whether it is influenced by specific mutations, the GppNHp·Mg^{2+} complexes with the p21 mutants G12D, Y32R, T35A, E62H, and S65P were studied. All of these residues are close to the nucleotide binding site in different structural elements. It turned out that the relative populations as well as the chemical shift parameters varied for each of the mutants. The parameters obtained are summarized in Table 1. Typical examples are shown in Figure 2. In the following we arbitrarily designate the conformational state where the β-resonance of the nucleotide is shifted downfield relative to the average β-position as state 1 and the state where the β-resonance of the nucleotide is shifted upfield relative to the average position as state 2. In the spectrum of p21(S65P) the two states are most clearly visible, the β-resonances are well separated, and the populations of the two states are almost equal. A similar result was obtained for p21(E62H), another mutant in loop L4 (spectrum not shown). In the spectrum of p21(G12D), a mutant in the phosphate binding loop L1, the two states are still visible, but state 1 now dominates. The spectrum of p21(T35A), a mutant in the effector loop L2, is peculiar. Only one rather narrow β-resonance line is visible at the position of the downfield shifted β-resonance in wild-type protein, suggesting that only one conformational state exists in this mutant. The same is true for p21(Y32R), but the spectral quality is not good enough to exclude the existence of state 2 with absolute certainty.

As in the case of the wild-type protein a possible dependence of the line splitting and/or the equilibrium constant K on the pH was tested for p21(S65P)·GppNHp·Mg^{2+} in the range from pH 5.5 to pH 8.9. Within the limits of error the splitting and the populations of the two states are again independent of pH in the range examined. Removal of the nucleotide-bound metal ion from the active center by addition of EDTA leads to a new set of phosphorus NMR lines of the bound nucleotide which is not identical to that for either of the two states. The β- and γ-phosphates are shifted upfield; the α-phosphate is shifted downfield (Table 1). The chemical shift positions of the two magnesium-free complexes examined, S65P·GppNHp and T35A·GppNHp, are very similar. From these spectra it cannot be decided whether two conformational states also exist in Mg^{2+}-free protein since signal overlap is quite severe and spectral quality is rather poor.

Calculation of the Equilibrium and Rate Constants by Complete Line-Shape Analysis. For the simulation of the exchange spectra, the *J*-coupling constants must be known. The *J*-coupling constants of GppNHp·Mg^{2+} were determined from phosphorus NMR spectra of free GppNHp·Mg^{2+} in D_2O at 10 °C and pH 7.2. The *J*-coupling values for phosphate−phosphate coupling are $^2J_{\alpha\beta} = 16.6$ Hz, $^2J_{\beta\gamma} = 8.2$ Hz, and $^4J_{\alpha\gamma} = 0$ Hz with an error $\Delta^2 J_{ij} < \pm 1$ Hz. These values were also taken as an approximation for the simulation of the spectra of the nucleotide−protein complexes (Figure 3). The estimation of the transverse relaxation times T_2 in the absence of exchange was especially difficult and was performed iteratively as described in Materials and Methods.

Table 1 shows that in the complex with wild type p21^{ras} the highfield-shifted state 2 is slightly favored although the equilibrium constant K is still very near to 1. Within the limits of error the populations of the two states in the mutant protein p21(S65P) are equal, which means that the forward and backward reaction rates k_1 and k_{-1} are equal. As is to be expected, the transverse relaxation rates are different for the different phosphate group spins since the number and spatial distribution of interacting spins in the environment of the ^{31}P nuclear spins vary. However, there are also differences between the transverse relaxation rates in complexes 1 and 2. The relaxation rates of the β- and γ-phosphorus are very similar and also change similarly in the two states, whereas the relaxation rate of the α-phosphate group is increased significantly (for data see legend to Figure 3). These relaxation rate differences also indicate structural differences in the close proximity of the phosphate groups in the two states. The temperature dependence of the NMR spectra reveals that the equilibrium constant K is not or only very weakly dependent on the temperature. This can also be seen qualitatively by comparing the ratio of the integrals of the β-phosphate lines at low temperatures with the weighted line position of the averaged β-phosphate line at

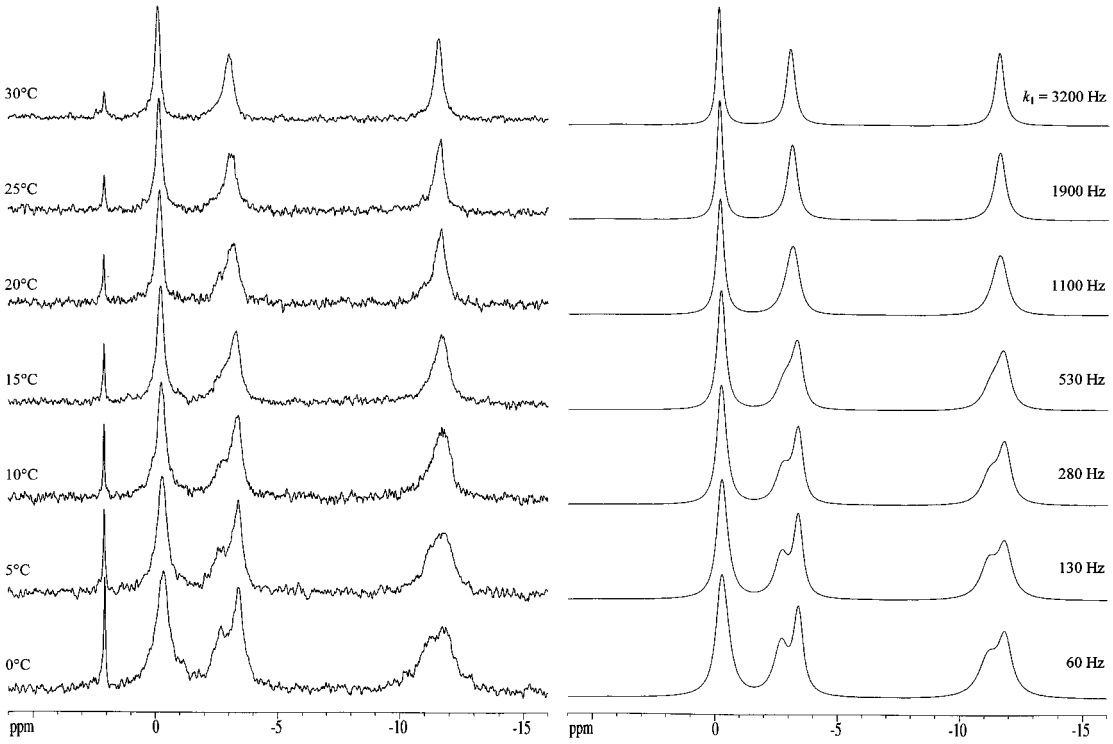

FIGURE 3: Experimental and simulated ^{31}P NMR spectra of p21^{ras}(wt)·GppNHp·Mg^{2+} at different temperatures: (left) experimental data; (right) simulated data. The chemical shift values used for the simulation of the experimental data are given in Table 1, and the $^2J_{PP}$ coupling constants were taken from free GppNHp·Mg^{2+} ($^2J_{\alpha\beta}$ = 16.6 Hz, $^2J_{\beta\gamma}$ = 8.2 Hz, and $^4J_{\alpha\gamma}$ = 0 Hz). The calculated transverse relaxation rates $1/T_2$ in the absence of exchange at 20 °C are 286, 205, 217, 136, 227, and 147 s^{-1} for the $\alpha^{(1)}$-, $\alpha^{(2)}$-, $\beta^{(1)}$-, $\beta^{(2)}$-, $\gamma^{(1)}$-, and $\gamma^{(2)}$-resonances. They were determined as described in Materials and Methods.

Table 2: Exchange Rates k_1 for the Two Conformational States in p21^{ras}(wt)·GppNHp·Mg^{2+} and p21^{ras}(S65P)·GppNHp·Mg^{2+} at pH 7.4[a]

p21^{ras}·GppNHp·Mg^{2+}									
temp (°C)	0	5	10	15	20	25	30	32	37
experimental rate k_1 (Hz)	60	130	280	530	1100	1900	3200		
calculated rate k_1 (Hz)	64	133	267	522	993	1854	3421	4304	7691
p21^{ras}(S65P)·GppNHp·Mg^{2+}									
temp (°C)	0	5	10	15	20	25	30	32	37
experimental rate k_1 (Hz)		95		550		2000		3800	
calculated rate k_1 (Hz)	52	105	223	452	892	1746	3248	4291	7618

[a] Experimental rate constants were determined from ^{31}P NMR spectra by line-shape simulations as described in Materials and Methods; theoretical rate constants were calculated from the fit of these data to the Eyring equation (8).

Table 3: Activation Energies in p21^{ras}(wt)·GppNHp·Mg^{2+} and p21^{ras}(S65P)·GppNHp·Mg^{2+} at pH 7.4[a]

	temp (°C)	$\Delta G^{\ddagger}$ (kJ/mol)	$\Delta H^{\ddagger}$ (kJ/mol)	$\Delta S^{\ddagger}$ (kJ/mol)
p21^{ras}(wt)·GppNHp·Mg^{2+}	5	60.2 ± 6	88.5 ± 2	102 ± 20
	20	58.6 ± 6		
	37	57.2 ± 7		
p21^{ras}(S65P)·GppNHp·Mg^{2+}	5	54.3 ± 12	92.7 ± 7	138 ± 30
	20	53.4 ± 12		
	37	51.1 ± 13		

[a] Free activation enthalpy $\Delta G^{\ddagger}$, activation enthalpy $\Delta H^{\ddagger}$, and activation entropy $\Delta S^{\ddagger}$ were calculated as described in Materials and Methods from the data shown in Figures 3 and Table 2.

high temperature (Figure 3). The exchange rates obtained for the wild-type protein and the mutant p21(S65P) by complete line-shape analysis are rather similar (Table 2). The activation enthalpies and activation entropies obtained from the fit of the data to the Eyring equation (Figure 4) may differ by a small amount; however, this is not significant at the error level (Table 3).

^{31}P NMR Spectra of p21·GTP·Mg^{2+} Complexes. An important question is whether the two states of p21^{ras} observed for the nonhydrolyzable GTP analog GppNHp also exist for GTP itself. One problem for such measurements is the hydrolysis of GTP during the relatively lengthy NMR experiments. ^{31}P NMR measurements of the GTP·Mg^{2+} complex with wild-type p21 at 202 MHz showed no clear indication that a second conformation exists although the β-resonance appears to be somewhat broadened. Since in the GTP complex the exchange correlation time could be smaller (that is, the activation energy could be smaller), additional experiments were performed at a lower magnetic field corresponding to a ^{31}P resonance frequency of 146 MHz and a higher magnetic field corresponding to a resonance frequency of 243 MHz. No strong frequency dependence of the line width of the β-resonance of GTP could be observed, excluding a significant exchange contribution to

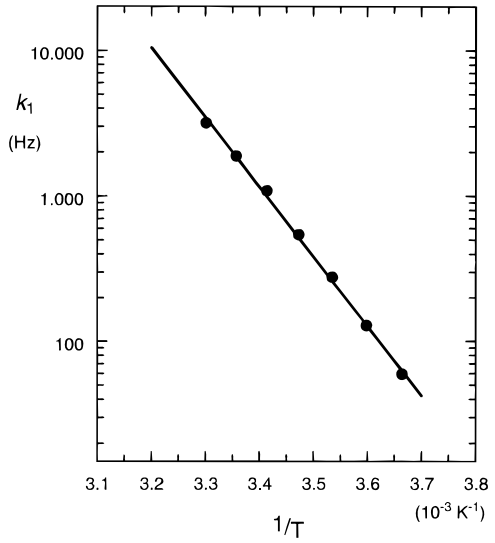

FIGURE 4: Eyring plot of the exchange rates vs the absolute reciprocal temperature for p21^{ras}(wt)·GppNHp·Mg^{2+}. The exchange rates derived from the NMR data were fitted to the Eyring equation with the activation enthalpy $\Delta H^{\ddagger}$ and the activation entropy $\Delta S^{\ddagger}$ as free parameters. The obtained parameters are summarized in Table 3.

the line width. In another set of experiments the freezing point of the solution was decreased by addition of glycerol (20% end concentration), and measurements were performed at −10 °C. Again no splitting of the resonance lines could be observed.

In p21^{ras}·GTP, besides an increased exchange rate, two other factors could impede the detection of the two states observed in the GppNHp complex: a decrease of the line separation or a large change of the equilibrium constant between the two states. Since we have observed changes of the line separation as well as the populations in p21 mutants, it was necessary to examine the GTP complexes of various mutants. In the spectra of the mutants p21(G12V) and p21(S65P) no indication of a second state was found as in the wild-type spectra. However, in the spectra of p21(Q61H) and p21(Q61L) a second weak peak was observed which was shifted upfield to the main β-resonance by 0.7 ppm to 0.8 ppm (Figure 5). As to be expected for two states in exchange, and as seen for the GppNHp complexes, the lines broaden with increasing temperature until at high temperature only one line is visible. Thus the second peak could represent the presumed second state; the relative population would be rather low with approximately 17% of the total signal intensity (Table 1). Magnesium binding usually leads to a downfield shift of the β-resonances of GTP. One possibility to explain the second resonance would be that it represents GTP bound to the metal-free p21−nucleotide complex. This explanation could be ruled out experimentally by addition of EDTA to the solution. Complexing of the Mg^{2+} ion leads to a much larger upfield shift of the β-resonance of the protein-bound nucleotide (by 1.6 ppm) and a downfield shift of the α- and γ-resonances by 0.6 and 2.6 ppm, respectively. The chemical shifts obtained for the GTP complexes with wild-type and mutant p21^{ras} are summarized in Table 1 together with the data for the GTP analog GTPγS with wild-type protein. In the latter case no indication of a second conformational state of the protein was observed.

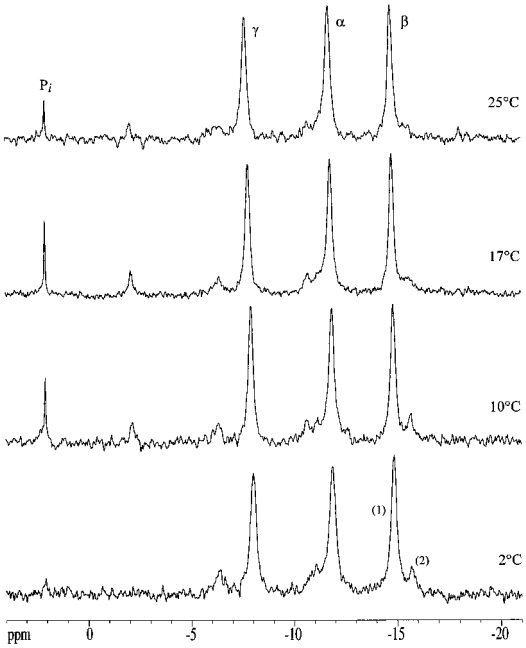

FIGURE 5: ^{31}P NMR spectra of p21^{ras}(Q61H)·GTP·Mg^{2+} at different temperatures: 0.8 mM protein in D_2O, pH 7.4. Note that the weak signals at −2.1 and −11.0 ppm originate from the hydrolysis product p21^{ras}(Q61H)·GDP·Mg^{2+} and the weak signals at −6.3 and −10.7 ppm represent free GDP·Mg^{2+}.

The highfield-shifted β-phosphate peak of the nonhydrolyzing mutant Q61H complexed with GTP·Mg^{2+} was found reproducibly in all preparations. Again, the relative populations and the splitting were independent of the Mg^{2+} concentration and the pH value, as observed for the GTP analog GppNHp. Analysis of the data leads to an equilibrium constant of $K = 0.21$ for the two states, clearly different from the value of approximately 1 found for the GppNHp complexes. The signal-to-noise ratio of the data was not sufficient for a determination of the rate constants by a complete line-shape analysis. However, the exchange rates and activation parameters are probably rather similar to those obtained for the GppNHp complexes, based on peak separation and the temperature dependence of the line widths.

EPR Spectroscopy of p21 Complexed with GppNHp·Mn^{2+}. As in most biological systems, in p21^{ras} Mn^{2+} ions can substitute for Mg^{2+}. Since manganese is paramagnetic, the metal ion can be observed directly by electron paramagnetic resonance (EPR) spectroscopy. The manganese EPR spectrum is very sensitive to changes in the coordination sphere of the metal ion [see, e.g., Kalbitzer (1987)]. The resolution

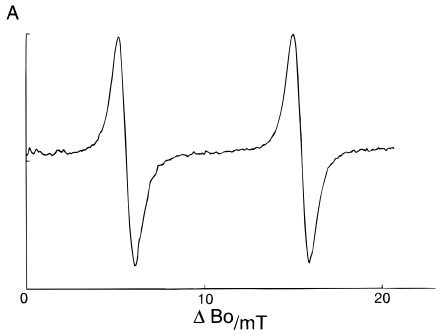

FIGURE 6: Low-field part of a 95 GHz EPR spectrum of p21^{ras}(wt)·GppNHp·Mn^{2+}. Only the two lowest field hyperfine lines ($m_I = 5/2$, $m_I = 3/2$) of the $m_S = +1/2$ to $-1/2$ transition are depicted. The temperature during the measurement was 1 °C; the sample volume was approximately 0.1 μL. The spectrum is an average of 50 slow adiabatic field scans. The line width of one hyperfine line is as narrow as 0.85 mT for this high Zeeman field of 3.4 T.

Table 4: Titration Parameters of GDP·Mg^{2+} and GppNHp·Mg^{2+} Complexes with p21^{ras}(E62H) and p21^{ras}(E63H)[a]

		p21^{ras}(E62H) GDP·Mg^{2+}					p21^{ras}(E63H) GDP·Mg^{2+}					p21^{ras}(E63H) GppNHp·Mg^{2+}				
residue	atom	δ_{A1}[b]	pK_1	δ_{AH}	pK_a	δ_{A^-}	δ_{A1}	pK_1	δ_{AH}	pK_a	δ_{A^-}	δ_{A1}	pK_1	δ_{AH}	pK_a	δ_{A^-}
His-27	$H^{\delta 2}$			7.50	6.7	7.09			7.50	6.6	7.09			7.50	6.4	7.07
	$H^{\epsilon 1}$			8.77		7.75			8.77		7.74			8.77		7.74
His-62/3	$H^{\delta 2}$	7.26	5.0	7.32	6.7	6.97	7.19	5.1	7.27	6.9	6.92	—[c]		—[c]	6.7	—[c]
	$H^{\epsilon 1}$			8.59		7.65			8.64		7.69	8.59				7.64
His-94	$H^{\delta 2}$			7.55	6.4	7.03			7.57	6.3	7.03	7.54		6.1		7.00
	$H^{\epsilon 1}$			8.59		7.75			8.61		7.76	8.67				7.75
His-166	$H^{\delta 2}$			6.96	7.1	6.60			6.96	7.1	6.60	6.95		7.1		6.60
	$H^{\epsilon 1}$			8.65		7.56			8.65		7.57	8.65				7.60

[a] The protein was dissolved in 6 mM phosphate buffer with D_2O and measured at 23 °C. Data were fitted to the modified Henderson−Hasselbalch equation [see, e.g., Hausser and Kalbitzer, (1991)]. [b] Chemical shift values δ_{A1}, δ_{AH}, and δ_{A^-} are in ppm, referenced to internal DSS. [c] Resonance line not identified.

of EPR spectra of protein bound manganese usually increases with the magnetic field since the line widths decrease. Figure 6 shows a part of a high-field EPR spectrum of the wild-type p21·GppNHp·Mn^{2+} complex recorded at 95 GHz. Even at this very high field of 3.4 T (the maximum field strength of a commercial Q-band EPR spectrometer is around 1.2 T), there is no indication of two conformational states influencing the coordination sphere of the metal ion.

^{1}H NMR of Histidine Mutants of p21. If there are two almost equally populated states, the two states might also be observable in ^{1}H NMR spectra in slow exchange, although this is not necessarily so since the slow exchange condition also depends on the line separation in the two states. Loop L4 is near the nucleotide binding site, and conformational changes in this region are not unlikely; also, the temperature factors in this region are indeed very high with up to 60 Å^2. Signals from histidine ring protons are easy to detect in ^{1}H NMR spectra and could serve as reporter groups for different conformational states in loop L4. We have studied three mutants, p21(Q61H), p21(E62H), and p21(E63H), by homonuclear TOCSY spectra of the GppNHp-bound proteins dissolved in D_2O. In the temperature range from 5 to 25 °C for all mutants no indication of a splitting of the histidine resonance lines could be observed.

Since the lifetime as well as the chemical shift differences of the two conformational states could be pH dependent, the pH of the sample was varied in the range from pH 4 to pH 9.2. Again, in the whole pH range no indication of a splitting of the resonance lines of His-63 could be observed. As a side effect the titration parameters for the histidine residues could be calculated (Table 4). However, at lower temperatures the resonance lines of His-27 in the spectra of the two mutants are much broader than those of the other histidine residues, suggesting a possible exchange broadening of this line. Since the two states found by ^{31}P NMR of the GppNHp complexes could also exist in the GDP state, the titration experiments were performed for p21(E62H)·GDP·Mg^{2+} and p21(E63H)·GDP·Mg^{2+} [titration values for Q61H were published by Schlichting et al. (1990a)]. At neutral pH no line splitting was observed for the histidine resonance, although the resonance line of His-27 is again broader than that of the other residues. However, below pH 5.5 the $H^{\epsilon 1}$-resonances of the histidine residues of loop L4 of the two mutants doubled with a commitant change of the line intensities with pH. The equilibrium of the two states changed with pH; the process itself was fully reversible, the initial spectrum being obtained on increasing the pH above 5.5. Again, these experiments allowed the determination of the titration parameters of these residues (Table 4).

p21 Complexed with Raf-RBD. The Ras binding domain (RBD) of the effector protein c-Raf-1, Raf-RBD, binds tightly to p21^{ras} in the triphosphate form (K_d = 18 nM) as shown by Herrmann et al. (1996). Figure 7 shows the effect of p21·GppNHp·Mg^{2+} on the ^{31}P spectra when Raf-RBD is added in increasing amounts. The main effect is the disappearance of one of the two β-resonances of p21 in the complex. At a molar ratio of 1, only a single well-defined resonance remains at the chemical shift position assigned earlier to state 2. Raf-RBD seems to stabilize this conformation. The downfield-shifted β-resonance of p21^{ras} appears to have vanished at a molar ratio of 0.5 of Raf-RBD to Ras. However, if Raf-RBD were to bind only to state 2 of Ras, one would expect precisely such an effect, since at this molar ratio state 1 should only contribute 24% of the β-phosphate signal. The corresponding signal should only be visible as inhomogeneous broadening of the β-phosphate resonance, as is indeed observed.

An increase of all line widths by a factor of 1.4 would be expected in the complex when the line widths would be dominated by dipolar interaction modulated by the rotational diffusion of the complex. However, as already noted, the Ras spectrum is exchange broadened. If we assume that in the Ras·Raf complex the exchange broadening can be neglected, the increase of the line width corresponds closely to the values calculated using the corrected transverse

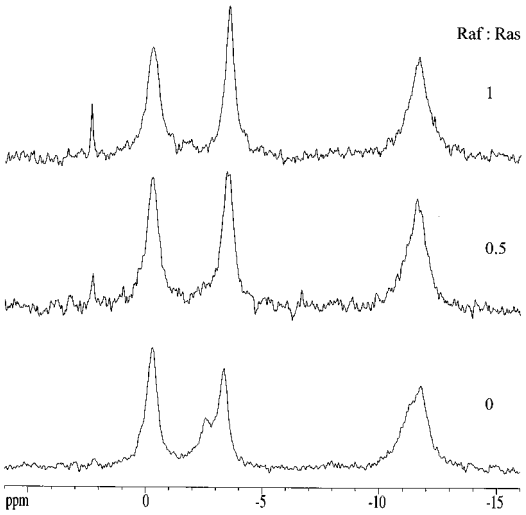

FIGURE 7: Concentration series of p21^{ras}(wt)·GppNHp·Mg^{2+} complexed with Raf-RBD. The ^{31}P NMR spectra were recorded at a temperature of 5 °C, pH 7.4, in D_2O. The Raf-RBD : p21^{ras} ratio varies between 0 (bottom spectrum) and 1 (top spectrum), starting with a solution of ~1.1 mM p21. Note that the high Ras·Raf affinity (K_d = 18 nM) leads to full formation of the complex.

Scheme 1

$$\begin{array}{ccccc} p21^{(1)}\cdot GppNHp\cdot Mg^{2+} + GAP & \underset{k_{-1}^{(1)}}{\overset{k_1^{(1)}}{\rightleftharpoons}} & p21^{(1)}\cdot GppNHp\cdot Mg^{2+}\cdot GAP & \underset{k_{-2}^{(1)}}{\overset{k_2^{(1)}}{\rightleftharpoons}} & p21^{(1)}\cdot GAP + GppNHp\cdot Mg^{2+} \\ k_1^{(12)}\downarrow\uparrow k_{-1}^{(12)} & & k_2^{(12)}\downarrow\uparrow k_{-2}^{(12)} & & k_3^{(12)}\downarrow\uparrow k_{-3}^{(12)} \\ p21^{(2)}\cdot GppNHp\cdot Mg^{2+} + GAP & \underset{k_{-1}^{(2)}}{\overset{k_1^{(2)}}{\rightleftharpoons}} & p21^{(2)}\cdot GppNHp\cdot Mg^{2+}\cdot GAP & \underset{k_{-2}^{(2)}}{\overset{k_2^{(2)}}{\rightleftharpoons}} & p21^{(2)}\cdot GAP + GppNHp\cdot Mg^{2+} \end{array}$$

relaxation rates given in the legend of Figure 3. This interpretation is also supported by the observed temperature dependence of the line widths and chemical shifts. An increase of the temperature up to 25 °C in four steps shows the typical temperature dependence of the line widths according to eq 7 in absence of exchange (data not shown). Within the limits of error the chemical shift values for the complex are independent of the temperature (Table 5).

p21 Complexed with GAP. Two sets of experiments were performed to study the interaction of p21·GppNHp·Mg^{2+} with the catalytic domain GAP-334 of the GTPase activating protein p120-GAP (Gideon et al., 1992). First, the relative concentration of p21 to GAP was varied at a fixed temperature of 5 °C. In the second series of experiments the temperature dependence of the ^{31}P NMR spectra of the complex and the change of the kinetic parameters with temperature were studied. Taking the two conformational states, 1 and 2 of the p21·GppNHp·Mg^{2+} complex into account, the kinetic scheme for the description of the equilibrium in solution can be written as shown in Scheme 1. Since the binding constant of p21 and its complex with GAP for GppNHp·Mg^{2+} is rather high (> 10^{11} M^{-1} at 5 °C; John et al., 1990), the contributions of free nucleotide to the ^{31}P spectrum can be neglected at concentrations of the nucleotide smaller than the concentration of p21. Figure 8 shows that in accordance with this expectation the addition of GAP does not lead to a release of the nucleotide from the protein. The chemical shifts in the complex of p21(wt)·GppNHp·Mg^{2+} with GAP are rather similar to the shifts in uncomplexed p21·GppNHp·Mg^{2+} (Table 5), indicating that no major structural rearrangement near the phosphate groups occurs after binding to GAP. The splitting of the β-resonance line disappears on addition of GAP to Ras. After saturation with GAP only one homogeneous line remains at low temperature (5 °C). The remaining β-phosphate signal, which initially is located exactly midway between the two split lines, shifts somewhat downfield on increasing the temperature.

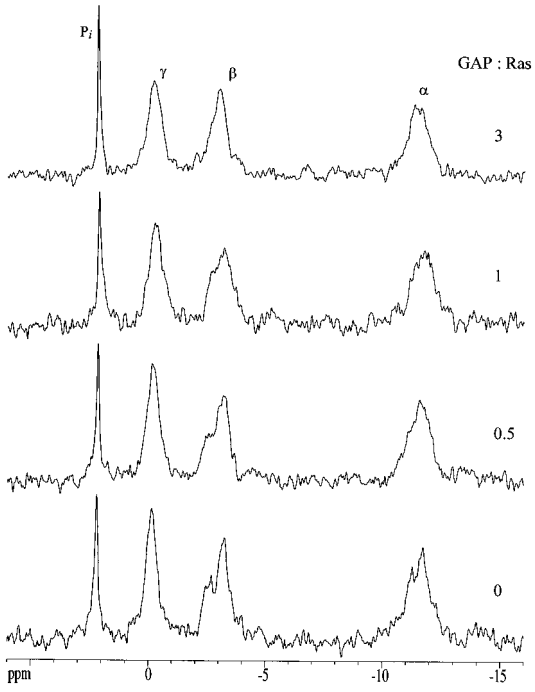

FIGURE 8: ^{31}P NMR spectra of p21^{ras}(wt)·GppNHp·Mg^{2+} complexed with GAP-334. The pH has been adjusted to 7.4 in D_2O at a temperature of 5 °C. The molar ratio between GAP and p21 (K_d = 21 μM) was varied by addition of a concentrated solution of 0.7 mM GAP (23 mg/mL) and was varied between 0 (bottom spectrum) and 3 (top spectrum).

The molecular mass of the p21^{ras}·GAP complex is 2.7-fold greater than that of p21 alone, so one would expect 2.7-fold larger line widths in the complex if the rotational correlation time of the complex alone determines the line widths. However, the ^{31}P NMR line widths in the complex are only slightly larger than in p21 alone (Figure 8). A possible explanation for these observations is that in the complex the exchange broadening is strongly reduced or no longer exists at all. At higher temperature (Figure 9) the ratio of the line widths of the γ-resonance in free and complexed p21 is close to the theoretical ratio of 1:2.7, indicating that at this temperature exchange broadening for the γ-resonance can be neglected. Also, the relatively small change of the line widths of all phosphorus resonances with temperature agrees with the change of the rotational correlation time expected from the corresponding viscosity change (eq (5) of the solution (Figure 9): this means that exchange broadening does not play an important role in the p21^{ras}·GAP complex.

Since two different spectra can be observed both for uncomplexed p21 and for p21 complexed with GAP (Figure 8), the slow exchange condition $|\Delta\omega\tau_e| \gg 1$ applies. From the peak separation $\Delta\omega$ one obtains a lower limit for the lifetime of the p21·GAP complex of 1.8 ms in state 1 and 3.4 ms in state 2. The rate constants for the dissociation of GAP from the complex are therefore less than $k_{-1}^{(1)} < 570$

Table 5: Chemical Shift Values from ^{31}P NMR Spectra of p21^{ras} Complexed with Raf-RBD or GAP-334 at Different Temperatures[a]

protein complex	temp (°C)	chemical shifts δ (ppm)[b] α	β	γ
Raf-RBD complexed with p21(wt)·GppNHp·Mg^{2+}	5	−11.7	−3.6	−0.3
	15	−11.7	−3.6	−0.3
	25	−11.7	−3.6	−0.3
GAP complexed with p21(wt)·GppNHp·Mg^{2+}	5	−11.5	−3.0	−0.2
	10	−11.4	−2.9	−0.1
	20	−11.4	−2.7	−0.0
GAP complexed with p21(Q61L)·GTP·Mg^{2+}	5	−11.9	−14.9	−8.0
	15	−11.9	−14.9	−7.8
	25	−11.8	−14.8	−7.6

[a] Measurements were performed at pH 7.4. [b] The error of the chemical shift determination is $\Delta\delta < \pm 0.1$ ppm.

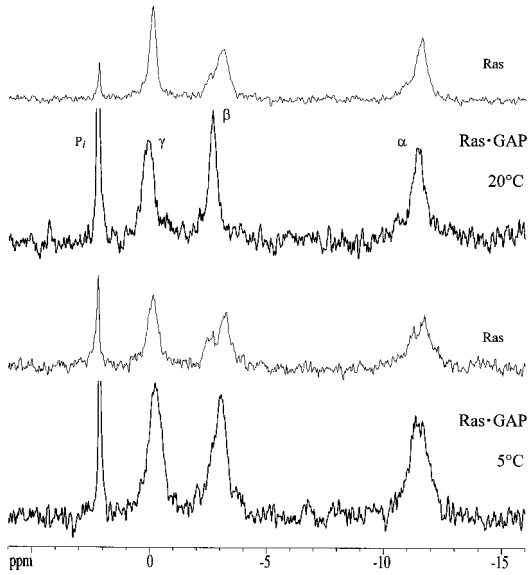

FIGURE 9: ^{31}P NMR spectra of p21^{ras}(wt)·GppNHp·Mg^{2+} complexed with GAP-334 at different temperatures. The molar ratio of GAP to p21 was 3:1; sample conditions were as in Figure 8. The temperature was varied between 5 and 20 °C. For comparison, the spectra of noncomplexed Ras are shown as lighter curves above.

s^{-1} and $k_{-1}^{(2)} < 290\ s^{-1}$, respectively. Assuming that the dissociation constant $K_d = 21\ \mu M$ (Gideon et al., 1992) applies for the two states, the on-rates can be calculated as $k_1^{(1)} < 27\ \mu M^{-1}\ s^{-1}$ and $k_1^{(2)} < 14\ \mu M^{-1}\ s^{-1}$. The line position of the α-resonance in the GAP complex is independent of temperature, but a significant downfield shift can be observed with increasing temperature for the β- and γ-resonance lines (Table 5). A similar result concerning chemical shift values and line width was obtained for the complex of GAP with p21 in the presence of its natural substrate GTP in the slow hydrolyzing mutant Q61L. The chemical shifts are very close to the values obtained in the absence of GAP (Table 5), the lines being shifted only slightly downfield with increasing temperature.

DISCUSSION

The Two Conformational States of the p21−Nucleoside Triphosphate Complex. The NMR data show unequivocally that p21^{ras} exists in two conformational states which are sensed by the phosphate atoms of GppNHp·Mg^{2+} bound to the active site. In the wild-type protein the populations of the two states are almost equal, the corresponding equilibrium constant $K_1^{(12)}$ being close to 1. Mutations in loop L4 (E62H or S65P) do not influence this equilibrium very much. In contrast, mutations in the phosphate binding loop (G12D) or the effector loop (Y32R or T35A) stabilize conformational state 1 (Figure 2). The activation enthalpies for the conformational transition of the wild-type protein and the mutant p21(S65P) are rather high (89 and 93 kJ mol^{-1}) and do not differ within experimental error. For comparison, transient opening of one hydrogen bond would have an activation energy of the order of 20 kJ mol^{-1}. This indicates that a larger conformational transition close to the phosphate moieties of the nucleotides takes place, such as local structural transitions and slight rearrangements of the surrounding loops.

The two states observed in the complex with the nonhydrolyzable analog GppNHp probably also exist in complexes with the natural substrate GTP. At least in the oncogenic mutants Q61H and Q61L an additional peak for the β-phosphate group could again be identified with characteristics similar to those observed for the GppNHp complexes. The upfield shift of the additional peak, approximately 0.7 ppm, is close to the values found for GppNHp, and a qualitative analysis of the temperature dependence of the spectra shows that also the activation enthalpies involved are rather similar to those observed for the GppNHp complexes. However, the equilibrium constant $K_1^{(12)}$ is influenced by the nature of the nucleotide, where state 1 is much preferred in the GTP complex.

Structural Basis of the Two Conformational States. The two structural states found by NMR were not identified in X-ray crystallographic studies. In general, it is very difficult to interpret phosphorus chemical shift changes in structural terms. However, a wealth of X-ray structures of GppNHp complexes with wild-type and mutant p21 exists which can help in interpreting the data. From these data there are no hints that two different conformational states involve the nucleotide itself or its direct ligands. The EPR data presented here also make it unlikely that the two states involve the direct environment of the metal ion or represent different coordination schemes of the metal−nucleotide complex. When direct effects involving conformational states of the nucleotide are unlikely, the most plausible explanation for the shift differences is a difference in the anisotropy of the magnetic susceptibility of a nearby group in the two states.

Chemical shift changes of the order of 1 ppm are often found close to aromatic ring systems (ring current shifts). The ^{1}H NMR experiments on the loop L4 mutants give no indication of a larger structural change in this region. However, an obvious candidate is Tyr-32 in the effector loop L2 of p21^{ras} which seems to be flexible since it has different positions relative to the phosphate groups in different crystal structures (Table 6). In crystal structures of GppNHp complexes of p21^{ras}(1−166) it often interacts with the neighboring p21 molecule via crystal packing forces (Pai et al., 1990; Krengel et al., 1990). Correspondingly, it is relatively far (>0.9 nm) from the β-phosphate of its own molecule. In other structures it is found close to its own phosphates as in the structure of the G12D mutant (Franken et al., 1993) or of the wild-type protein complexed with caged GTP (Schlichting et al., 1990b). A structural model reflecting these differences is shown in Figure 10. The observed shifts in our experiments are between 0.7 and 0.9 ppm for the upfield-shifted state 2 in the triphosphate complexes. If the ring current of Tyr-32 were the dominant reason for the upfield shift of the β-resonance, the shift would not be observable in the mutant p21(Y32R) since no ring system is present. We indeed see only one β-resonance with chemical shift values typical for state 1 (Figure 2). Here, the line broadening at the high-field side could be caused by interaction of the positively charged guanidinium ion of Arg-32 with the negatively charged phosphate groups.

There is another report which supports our hypothesis that Tyr-32 may come close to the β-phosphate in state 2: in the structure of the GppNHp complex of a close relative of p21^{ras}, Rap1A, bound to the Ras binding domain of c-Raf-1, Raf-RBD, Tyr-32 comes close to the β-phosphate (0.5 nm) and forms a hydrogen bond with the γ-phosphate (Nassar et al., 1995). Rap1A is a small GTP-binding protein with an effector region identical to Ras and an overall sequence identity of 50% such that the complex between

Table 6: Orientation of the Nucleoside Phosphates Relative to the Center of the Tyr-32 Ring System in Various Structures of p21^{ras} [a]

	α-phosphate		β-phosphate		γ-phosphate	
structure	r (Å)[b]	ϑ[c] (deg)	r (Å)	ϑ (deg)	r (Å)	ϑ (deg)
p21^{ras}·GppNHp·Mg^{2+} (**1**)[d]	8.8	29.7	9.5	18.4	8.5	13.2
p21^{ras}(G12P)·GppNHp·Mg^{2+} (**2**)[e]	8.7	26.3	9.4	14.8	8.4	12.8
p21^{ras}(G12D)·GppNHp·Mg^{2+} (**3**)[f]	5.5	22.2	6.1	29.3	5.8	56.1
p21^{ras}·GDP·Mg^{2+} (**4**)[g]	7.4	68.0	8.1	72.8		
p21^{ras}·GDP·Mg^{2+} (**5**)[h]	8.4	78.0	8.9	82.9		
p21^{ras}·GppCH$_2$p·Mg^{2+} (**6**)[i]	8.8	30.0	9.3	18.9	8.3	14.0
p21^{ras}·GppCH$_2$p·Mg^{2+} (**7**)[j]	8.4	78.2	9.5	79.6	9.8	88.5
	5.6	26.0	5.7	36.2	5.5	64.9
p21^{ras}·cagedGTP·Mg^{2+} (**8**)[k]	9.7	26.8	6.9	17.6	4.1	28.0
Rap1A·GppNHp·Mg^{2+}·Raf-RBD (**9**)[l]	5.0	40.4	5.2	44.9	4.8	74.4

[a] Structures **1**−**7** were taken from the Brookhaven Protein Data Bank. [b] r is the length of a vector $\vec{r}$ joining the center of the phosphorus atom and the center of the tyrosyl ring. [c] ϑ is the angle between $\vec{r}$ and the orthogonal vector through the center of the tyrosyl ring plane. [d] Crystal structure from Pai et al. (1990). Resolution: 1.35 Å. [e] Crystal structure from Franken et al. (1993). Resolution: 1.5 Å. [f] Crystal structure from Franken et al. (1993). Resolution: 2.3 Å. [g] Crystal structure from Milburn et al. (1990). Resolution: 2.0 Å. [h] NMR solution structure from Kraulis et al. (1994); average RMSD value of the Cα atoms for loop L2: ∼1.2 Å. [i] Crystal structure from Krengel (1991). Resolution: 1.54 Å. [j] Crystal structure from Milburn et al. (1990). Resolution: 1.95 Å. The conformation of loop L2 varies for the four molecules in the asymmetric unit; the spread is denounced by two different orientations. [k] Refined crystal structure from Schlichting et al. (1990b). Resolution: 3.0 Å. [l] Crystal structure of the complex from Nassar et al. (1995). Resolution: 2.2 Å.

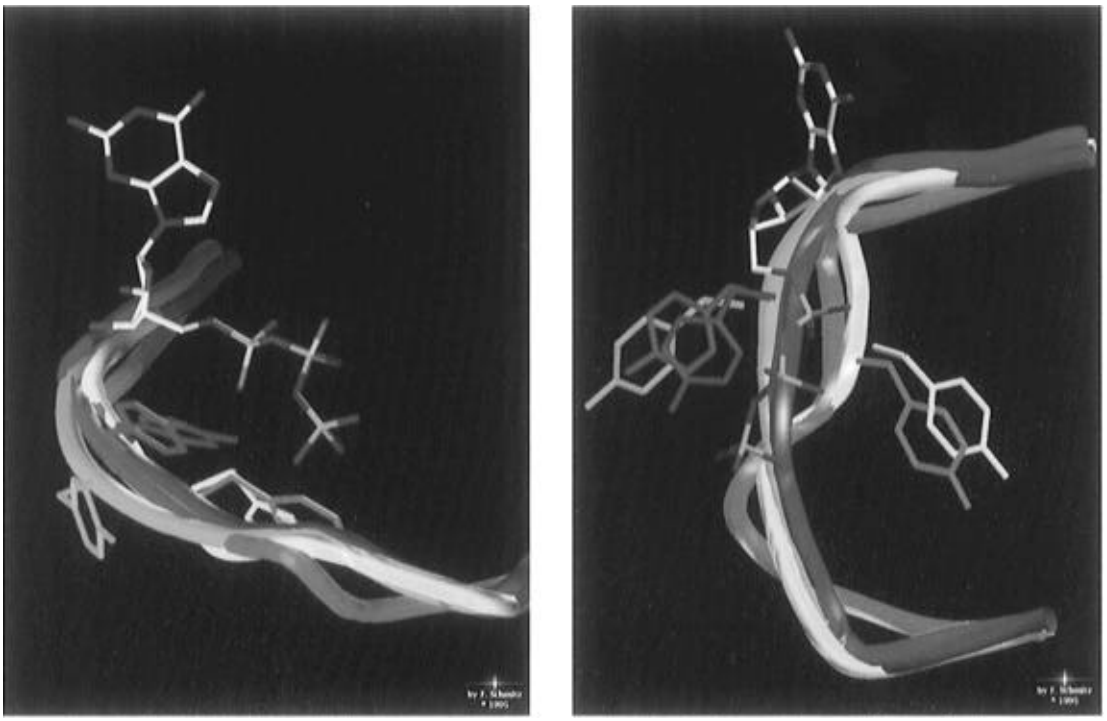

FIGURE 10: Atomic model of the nucleotide environment in different crystal structures. Two different views of the same superposed structures are depicted. The conformation of the effector loop L2 (backbone) and the orientation of the Tyr-32 ring system relative to the nucleoside phosphates are shown for p21^{ras}(wt)·GppNHp·Mg^{2+} (blue; Pai et al., 1990), the GppCH$_2$p·Mg^{2+} and GDP·Mg^{2+} complex (yellow and green; Milburn et al., 1990), the mutant G12D (cyan; Franken et al., 1993), and the complex of Rap1A·GppNHp·Mg^{2+}·Raf-RBD (red; Nassar et al., 1995). The structure alignment is based on the coordinates of the phosphorus atoms of the nucleotides. Note that in the structure of the Rap1A·Raf complex the ring system of Tyr-32 is very close to the β-phosphate moiety.

Raf-RBD and p21^{ras} is expected to be very similar. The nucleotide binding site of different crystal structures is shown in Figure 10. From the crystal structure coordinates of the Rap1A·GppNHp·Mg^{2+}·Raf-RBD complex (Table 6) the shifts expected for the phosphate resonances can be calculated. Using the Johnson−Bovey model (Johnson & Bovey, 1958) together with the empirical constants given by Perkins and Dwek (1980), one obtains additional shifts of only −0.16, −0.10, and +0.19 ppm for the α-, β-, and γ-resonances although the phosphate groups are rather close to the tyrosyl ring. However, the ring current shifts are also dependent on the relative orientations: if in the Ras complex the aromatic ring of Tyr-32 were rotated by only 20° about the $C_\beta-C_\gamma$ bond, the calculated values would explain nicely the observed changes of the chemical shifts in state 2.

Finally, this interpretation is in good agreement with the spectra recorded for the p21^{ras}·Raf-RBD complex, where the upfield shifted state 2 is stabilized (Figure 7). This might suggest that Ras binds the effector molecule only in state 2 with Tyr-32 in hydrogen bond contact to the γ-phosphate group. If the high-field shift difference of 0.72 ppm for the β-phosphate in state 2 were caused exclusively by the ring current of Tyr-32, the perpendicular distance from the ring center to the phosphorus atom would have to be 0.43 nm.

Interaction of p21 with GAP. Since the interaction of GAP with p21 is slow on the NMR time scale, upper limits for

the on- and off-rate constants of k_1 and k_{-1} could be determined from the NMR spectra. Although different off-rates could exist for the two conformational states, only state 1 can be observed unequivocally by NMR in the complex since the resonance line of the complex overlaps with the line of state 2 (Figure 8). The limits for the rate constants obtained for state 2 assume that slow exchange conditions apply also for this state. Since no large chemical shift changes are found, a direct interaction of functional groups of GAP with the phosphate moieties of the nucleotide of p21 (at least at the ground state of the reaction) is rather unlikely. Thus it is also unlikely that the GAP-mediated GTP hydrolysis involves a direct involvement of GAP in the chemical mechanism. As we were able to show earlier, the hydrolysis of GTP can be explained satisfactorily by a substrate-assisted catalysis (Schweins et al., 1995). In principle, the hydrolysis rate could be enhanced by electrostatic long-range interactions which would lead to an increase in the pK_a value of the γ-phosphate group. The active site of p21 with bound GTP is located at the protein surface. GAP could replace water molecules at the surface of the active site by binding to this region. As a result of this, the dielectric properties might change drastically and thereby induce catalytically favorable electrostatic interactions in the active site of p21.

From the data available one cannot define unequivocally the influence of GAP on the two conformational states of p21. The NMR spectra could be explained by two different basic models: (a) The binding of GAP leads to the stabilization of one of the states, so that only one signal of the β-resonance can be observed. (b) The binding of GAP leads to increased rates $k_2^{(12)}$ and $k_{-2}^{(12)}$ between the two states, so that only one averaged line would be observed in the complex. From the NMR data presented it is not possible to distinguish between the two mechanisms. However, if a conformational change of Tyr-32 were responsible for the observed chemical shifts, model b would predict that there is no strong interaction of Tyr-32 (and the effector loop) with GAP. With the assumption that the chemical shift values of the phosphorus resonances are essentially the same in free p21 and in the complex with GAP and that GAP has only an influence on the thermodynamics in the complex, model a would predict that the populations would change but the chemical shift values would be unchanged. At 5 °C this is clearly not true for the α- and β-resonance lines: the resonance positions observed for the complex are close to the weighted mean positions assigned to the two states in free p21 (Figure 9). In the GppNHp complex with equal populations of states 1 and 2, the weighted mean position corresponds to the center of the two lines. In the GTP complex the weighted mean position is close to the chemical shift value of the dominant state, 1. This is just the situation predicted by model b where the exchange between the two states (rate constants $k_2^{(12)}$ and $k_{-2}^{(12)}$) should be enhanced. At higher temperatures the line positions shift somewhat downfield to state 1, which corresponds to a change of the equilibrium constant $K_2^{(12)} = k_2^{(12)}/k_{-2}^{(12)}$ and thus favors model a.

If GAP enhances the exchange between the two states, we have to assume fast exchange even at 5 °C. The exchange rates can be approximated by line-shape simulations for the p21·GppNHp·Mg^{2+}·GAP complex by assuming the same simulation parameters as in Figure 3. The obtained rate constant $k_2^{(12)}$ at 25 °C is of the order of 10^5 s^{-1} compared to $k_1^{(12)} = 1900$ s^{-1} without GAP (see Scheme 1). This means an acceleration of the exchange process by a factor of 50−200 in the whole temperature range. These simulated rate constants are rather high, and since the natural line widths in the complex are most probably larger than the line widths of uncomplexed p21 used in the approximation, the exchange rates will be even higher. So, the question arises whether the conformational change including Tyr-32 could occur that fast at high temperature. As an upper limit one can estimate typical diffusion trajectories x in a time interval t of an isolated molecule with radius r using the Einstein−Smoluchowski equation for Brownian molecular motion $\langle x^2 \rangle = (kT/6\pi\eta r)t$. For a molecule with 0.6 nm radius—such as a side chain with an aromatic ring—the average motional diffusion in water in a time step of 10 μs (equal to $k_2^{(12)}$) is of the order of 63 nm at 25 °C. In our model a part of the effector loop L2, including Tyr-32, has to move at least 0.6 nm between the two states, which is still small compared to the distance possible in the simple molecular diffusion model. However, the dramatic increase in the exchange rates between the two states of p21 requires a decrease in the corresponding free activation enthalpies. It is likely that such a change in the free activation enthalpies involves also some structural changes in p21 (loop L2) itself. Such a change would lead to a change in populations (not only exchange rates) in the complex of Ras with GAP. The averaged chemical shift position of the β-resonance line in the complex does indeed change with the temperature: at low temperatures states 1 and 2 have similar populations, while at high temperatures only state 1 appears to be present (Figure 9).

CONCLUSION

From these results the following picture emerges: p21^{ras} can exist in two different conformations, which are characterized by structural transitions in loop L2 including Tyr-32. In state 1 Tyr-32 is far removed from the phosphate groups of the nucleotide; in state 2 it is rather close to these groups. In complexes with the nucleotide analog GppNHp the two states are almost equally populated, while in the presence of the physiological substrate GTP one state predominates, which therefore could trigger interacting proteins. The transition between the two states requires a relatively high activation enthalpy of approximately 90 kJ mol^{-1}, which corresponds closely to the reported activation enthalpy of GTP hydrolysis (Schweins et al., 1996). Interaction with GAP accelerates the exchange between the two states and shifts the equilibrium at higher temperature to state 1. The data suggest that GAP does not interact directly with the phosphate groups and has only subtle interactions with L2. In contrast, Raf-RBD interacts strongly with loop L2, stabilizes state 2, and probably preferentially binds to this state. This prediction could be tested by studying the binding kinetics of Raf-RBD to p21·GppNHp complexes.

ACKNOWLEDGMENT

We are grateful to Petra Gideon for providing the histidine mutants; also we thank Klaus Scheffzek, Roger S. Goody, and Ulrich Haeberlen for helpful discussions, John Wray for carefully reading the manuscript, and Kenneth C. Holmes for continuous support.

REFERENCES

Barbacid, M. (1987) *Annu. Rev. Biochem. 56*, 779−827.

Boguski, M. S., & McCormick F. (1993) *Nature 355*, 643−654.

Bradford, M. M. (1976) *Anal. Biochem. 72*, 248−254.

Brownbridge, G. G., Lowe, P. N., Moore, K. J., Skinner, R. H., & Webb, M. R. (1993*) J. Biol. Chem. 268*, 10914−10919.

Burgering, B. M., & Bos, J. L. (1995) *Trends Biochem. Sci. 20*, 18−22.

Campbell-Burk, S. (1989) *Biochemistry 28*, 9478−9484.

Campbell-Burk, S., Papastravos, M. Z., McCormick, F., & Redfield, A. G. (1989) *Proc. Natl. Acad. Sci. U.S.A. 86*, 817−820.

Eccleston, J. F., Moore, K. J., Morgan, L., Skinner, R. H., & Lowe, P. N. (1993*) J. Biol. Chem. 268*, 27012−27019.

Eyring, H. (1935) *J. Chem. Phys. 3*, 107−115.

Feuerstein, J., Kalbitzer, H. R., John, J., Goody, R. S., & Wittinghofer, A. (1987) *Eur. J. Biochem. 162*, 49−55.

Franken, S. M., Scheidig, A. J., Krengel, U., Rensland, H., Lautwein, A., Geyer, M., Scheffzek, K., Goody, R. S., Kalbitzer, H. R., Pai, E., & Wittinghofer, A. (1993) *Biochemistry 32*, 8411−8420.

Gideon, P., John, J., Frech, M., Lautwein, A., Clark, R., Scheffler, J. E., & Wittinghofer, A. (1992) *Mol. Cell Biol. 12*, 2050−2056.

Grand, R. J. A., Levine, B. A., Byrd, P. J., & Gallimore, P. H. (1989) *Oncogene 4*, 355−361.

Gutmann, D. H., Boguski, M., Marchuk, D., Wigler, M., Collins, F. S., & Ballester, R. (1993) *Oncogene 8*, 761−769.

Ha, J.-M., Ito, Y., Kawai, G., Miyazawa, T., Miura, K., Ohtsuka, E., Noguchi, E., Noguchi, S., Nishimura, S., & Yokoyama, S. (1989) *Biochemistry 28*, 8411−8416.

Hata-Tanaka, A., Kawai, G., Yamasaki, K., Ito, Y., Kajirura, H., Ha, J.-M., Miyazawa, T., Yokoyama, S., & Nishimura, S. (1989) *Biochemistry 28*, 9550−9556.

Hausser, K.-H., & Kalbitzer, H. R. (1991) *NMR in Medicine and Biology. Structure Determination, Tomography, In-Vivo Spectroscopy*, Springer-Verlag, Heidelberg.

Herrmann, C., Martin, G. A., & Wittinghofer, A. (1995) *J. Biol. Chem. 270*, 2901−2905.

Herrmann, C., Horn, G., Spaargaren, M., & Wittinghofer, A. (1996) *J. Biol. Chem. 271*, 6794−6800.

John, J., Schlichting, I., Schlitz, E., Rösch, P., & Wittinghofer, A. (1989) *J. Biol. Chem. 264*, 13086−13092.

John, J., Sohmen, R., Feuerstein, J., Linke, R., Wittinghofer, A., & Goody, R. S. (1990) *Biochemistry 29*, 6058−6065.

Johnson, C. E., & Bovey, F. A. (1958) *J. Chem. Phys. 29*, 1012−1014.

Kalbitzer, H. R. (1987) in *Metal Ions in Biological Systems* (Sigel, H., Ed.) Vol. 22, Marcel Dekker, Inc., New York and Basel.

Kaplan, J. I., & Fraenkel, G. (1980) *NMR of chemically exchanging systems*, Academic Press, New York.

Klaus, W., Schlichting, I., Goody, R. S., Wittinghofer, A., Rösch, P., & Holmes, K. C. (1986) *Biol. Chem. Hoppe-Seyler 367*, 781−786.

Kraulis, P. J., Domaille, P. J., Campbell-Burk, S. L., van Aken, T., & Laue, E. D. (1994) *Biochemistry 33*, 3515−3531.

Krengel, U. (1991) Dissertation, Universität Heidelberg.

Krengel, U., Schlichting, I., Scherer, A., Schumann, R., Frech, M., John, J., Kabsch, W., Pai, E. F., & Wittinghofer, A. (1990) *Cell 62*, 539−548.

Landolt-Börnstein (1969) *Zahlenwerte und Funktionen*, II/5a, Springer-Verlag, Berlin.

Larsen, R. G., Halkides, C. J., & Singel, D. J. (1993) *J. Chem. Phys. 98*, 6704−6721.

Latwesen, D. G., Poe, M., Leigh, J. S., & Reed, G. H. (1992) *Biochemistry 31*, 4946−4950.

Longo, P. A., Broido, M. S., Chen, J., Kung, H.-F., & Pincus, M. R. (1988) *Biochem. Biophys. Res. Commun. 157*, 776−782.

Lowe, P. N., & Skinner, R. H. (1994) *Cell. Signalling 6*, 109−123.

Lowy, D. R., & Willumsen, B. M. (1993) *Annu. Rev. Biochem. 62*, 851−891.

Milburn, M. V., Tong, L., de Vos, A. M., Brünger, A., Yamaizumi, Z., Nishimura, S., & Kim, S.-H. (1990) *Science 247*, 939−945.

Miller, A. F., Papastravros, M. Z., & Redfield, A. G. (1992) *Biochemistry 31*, 10208−10216.

Miller, A. F., Halkides, C. J., & Redfield, A. G. (1993) *Biochemistry 32*, 7367−7376.

Moore, K. J. M., Webb, M. R., & Eccleston, J. F. (1993) *Biochemistry 32*, 7451−7459.

Muto, Y., Yamasaki, K., Ito, Y., Yajima, S., Masaki, H., Uozumi, T., Wälchli, M., Nishimura, S., Miyazawa, T., & Yokoyama, S. (1993) *J. Biomol. NMR 3*, 165−184.

Nageswara Rao, B. D. (1989) *Methods Enzymol. 176*, 279−311.

Nassar, N., Horn, G., Herrmann, C., Scherer, A., McCormick, F., & Wittinghofer, A. (1995) *Nature 375*, 554−560.

Neal, S. E., Eccleston, J. F., & Webb, M. R. (1990) *Proc. Natl. Acad. Sci. U.S.A. 87*, 3562−3565.

Pai, E. F., Kabsch, W., Krengel, U., Holmes, K. C., John, J., & Wittinghofer, A. (1989) *Nature 341*, 209−214.

Pai, E. F., Krengel, U., Petsko, G. A., Goody, R. S., Kabsch, W., & Wittinghofer, A. (1990) *EMBO J. 9*, 2351−2359.

Perkins, S. J., & Dwek, R. A. (1980) *Biochemistry 19*, 245−258.

Press, W. H., Flannery, B. P., Teukolsky, S. A., & Vetterling, W. T. (1986) *Numerical Recipes. The Art of Scientific Computing*, Cambridge University Press, Cambridge.

Prisner, T. F., Rohrer, M., & Möbius, K. (1994) *Appl. Magn. Reson. 7*, 167−183.

Privé, G. G., Milburn, M. V., Tong, L., de Vos, A. M., Yamaizumi, Z., Nishimura, S., & Kim, S.-H. (1992) *Proc. Natl. Acad. Sci. U.S.A. 89*, 3649−3653.

Rensland, H., Lautwein, A., Wittinghofer, A., & Goody, R. S. (1991) *Biochemistry 30*, 11181−11185.

Rösch, P., Wittinghofer, A., Tucker, J., Sczakiel, G., Leberman, R., & Schlichting, I. (1986) *Biochem. Biophys. Res. Commun. 135*, 549−555.

Scheidig, A. J., Franken, S. M., Corrie, J. E. T., Reid, G. P., Wittinghofer, A., Pai, E. F., & Goody, R. S. (1995) *J. Mol. Biol. 253*, 132−150.

Schlichting, I., John, J., Frech, M., Chardin, P., Wittinghofer, A., Zimmermann, H., & Rösch, P. (1990a) *Biochemistry 29*, 504−511.

Schlichting, I., Almo, S. C., Rapp, G., Wilson, K., Petratos, K., Lentfer, A., Wittinghofer, A., Kabsch, W., Pai, E. F., Petsko, G. A., & Goody, R. S. (1990b) *Nature 345*, 309−315.

Schweins, T., Geyer, M., Scheffzek, K., Warshel, A., Kalbitzer, H. R., & Wittinghofer, A. (1995) *Struct. Biol. 2*, 36−44.

Schweins, T., Geyer, M., Kalbitzer, H. R., Wittinghofer, A., & Warshel, A. (1996) *Biochemistry* (submitted).

Skinner, R. H., Bradley, S., Brown, A. L., Johnson, N. J., Rhodes, S., Stammers, D. K., & Lowe, P. N. (1991) *J. Biol. Chem. 266*, 14163−14166.

Smithers, G. W., Poe, M., Latwesen, D. G., & Reed, G. H. (1990) *Arch. Biochem. Biophys. 280*, 416−420.

Tucker, J., Sczakiel, G., Feuerstein, J., John, J., Goody, R. S., & Wittinghofer, A. (1986) *EMBO J. 5*, 1351−1358.

Wiesmüller, L., & Wittinghofer, A. (1992) *J. Biol. Chem. 267*, 10207−10210.

Wittinghofer, A., & Herrmann, C. (1995) *FEBS Lett. 369*, 52−56.

Wittinghofer, A., Pai, E. F., & Goody, R. S. (1993) in *GTPases in Biology I* (Dickey, B. F., & Birnbaumer, L., Eds.) Chapter 14, Springer-Verlag, Berlin/Heidelberg.

Yamasaki, K., Kawai, G., Ito, Y., Muto, Y., Fujita, J., Miyazawa, T., Nishimura, S., & Yokoyama, S. (1989) *Biochem. Biophys. Res. Commun. 162*, 1054−1062.

Yamasaki, K., Shirouzu, M., Muto, Y., Fujita-Yoshigaki, J., Koide, H., Ito, Y., Kawai, G., Hattori, S., Yokoyama, S., Nishimura, S., & Miyazawa, T. (1994) *Biochemistry 33*, 65−73.

BI952858K